Rapid Communications

Emergence and persistence of flow inhomogeneities in the yielding and fluidization of dense soft solids

Vishwas Venkatesh Vasisht
Indian Institute of Technology Palakkad, Ahalia Integrated Campus, Kozhippara P. O, Palakkad, Kerala 678557, India and Department of Physics, Institute for Soft Matter Synthesis and Metrology, Georgetown University, 37th and O Streets, N.W., Washington, DC 20057, USA

Gabrielle Roberts
Department of Physics, University of Chicago, 5720 South Ellis Avenue, Chicago, Illinois 60637, USA

Emanuela Del Gado
Department of Physics, Institute for Soft Matter Synthesis and Metrology, Georgetown University, 37th and O Streets, N.W., Washington, DC 20057, USA

(Received 4 October 2017; revised 19 August 2019; accepted 25 May 2020; published 6 July 2020; corrected 22 July 2020)

In three-dimensional computer simulations of model non-Brownian jammed suspensions, we compute the time required to reach homogeneous flow upon yielding, by analyzing stresses and particle packing at different shear rates, with and without confinement. We show that the stress overshoot and persistent shear banding preceding the complete fluidization are controlled by the presence of overconstrained microscopic domains in the initial solids. Such domains, identifiable with icosahedrally packed regions in the model used, allow for stress accumulation during the shear startup. Their structural reorganization under deformation controls the emergence and the persistence of the shear banding.

DOI: 10.1103/PhysRevE.102.010604

Under shear, soft solids such as emulsions, foams, or colloidal pastes yield and eventually flow, a feature important from paints and food to pharmaceutical products and wet cements [1]. The shear stress increases with the strain γ and often overshoots before decaying towards a steady-state value that depends on the shear rate $\dot{\gamma}$. A major challenge to control the flow properties is that the evolution towards the steady state can be accompanied by spatial inhomogeneities, with only part of the material flowing and the rest remaining jammed [2–5]. Such a phenomenon, called shear banding, is well known to geologists and engineers but its origin and persistence in dense amorphous solids is largely not understood [1].

Advanced rheological and computational tools have gained new insights into inhomogeneous flows [2,5–14]. In various complex fluids, bands flowing at different rates are ascribed to flow-induced structuring or ordering transitions, and can survive in a steady state [15]. For dense soft solids, instead, flow inhomogeneities are thought to emerge from the relaxation of stress heterogeneities elastically stored in the material during the stress overshoot, which can significantly delay the onset of a homogeneous flow [2,3,11,16–19]. It has been shown that the age of the sample, which controls frozen-in stresses, has an impact on the stress overshoot [5,12] and that the competition between aging and flow-induced rejuvenation may lead to shear banding [20–22]. However, microscopic mechanical heterogeneities remain elusive to pin down, making it even harder to elucidate their possible role during the startup flow.

Here, we identify the link between the shear banding and its persistence in soft solids and the presence of stiffer, locally overconstrained domains. We use computer simulations of model dense non-Brownian suspensions where we can associate the overconstrained domains to the predominantly dodecahedral geometry of the Voronoi volumes, corresponding to a prevalently icosahedral particle packing. Such domains allow for stress accumulation during the stress overshoot and organize in space into a nonflowing band as shear stresses relax after the overshoot. The progressive, slow erosion of the nonflowing band helps reorganize the mechanical constraints in the material, eventually leading to its complete fluidization.

Our model soft solid is a non-Brownian suspension of volume fraction $\phi \approx 70\%$, consisting of 10^5 (97 556, unless otherwise specified) particles, with repulsive effective interactions mimicked via a truncated and shifted Lennard-Jones potential [23], whose strength ϵ is the unit energy in the simulations. The diameters of the particles are drawn from a Gaussian distribution with a variance of 10%, whose mean is used as unit length a. Albeit simple, the model captures the essential features of sheared soft solids [5,14,24–27]. We prepare the initial samples from a high-temperature dense liquid, cooled to low temperature using a NVT molecular dynamics (MD) protocol with a cooling rate Γ varying from 5×10^{-2} to $5 \times 10^{-6} \epsilon/(k_B \tau_0)$ (where $\tau_0 = a\sqrt{m/\epsilon}$ is the MD time unit with m the particle mass, and for the lowest Γ we perform 10^9 MD steps). Each sample is subsequently brought to the closest energy minimum and to $k_B T/\epsilon \simeq 0$ via energy

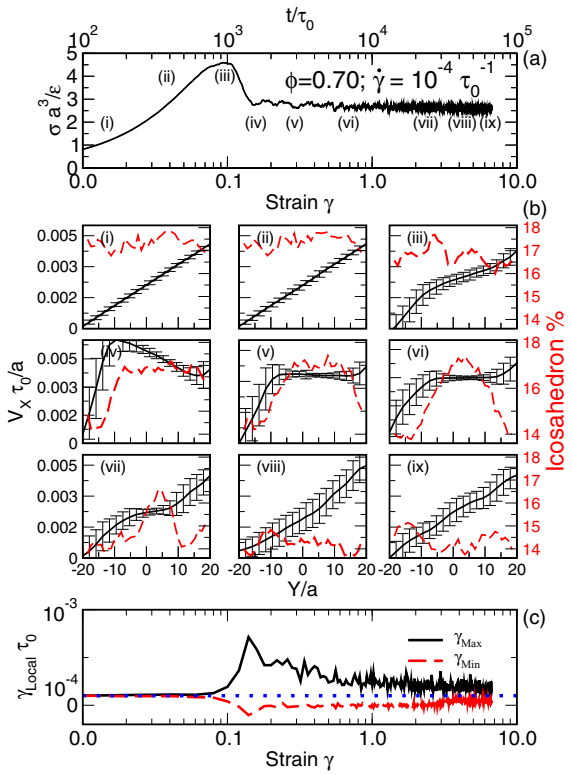

FIG. 1. (a) The load curve at $\dot{\gamma} = 10^{-4}\tau_0^{-1}$ for a system prepared at $\phi = 0.70$ with cooling rate $\Gamma = 5 \times 10^{-4}\epsilon/(k_B\tau_0)$. (b) The velocity profiles (solid line) at points (i)–(ix) of the load curve. The error bars are from sample-to-sample fluctuations for three samples. The dashed lines are the percentages of icosahedral packing. (c) The maximum (solid line) and minimum (dashed line) of the local shear rate (the numerical derivative of the velocity profile), along with the applied shear rate (dotted line), as a function of the strain.

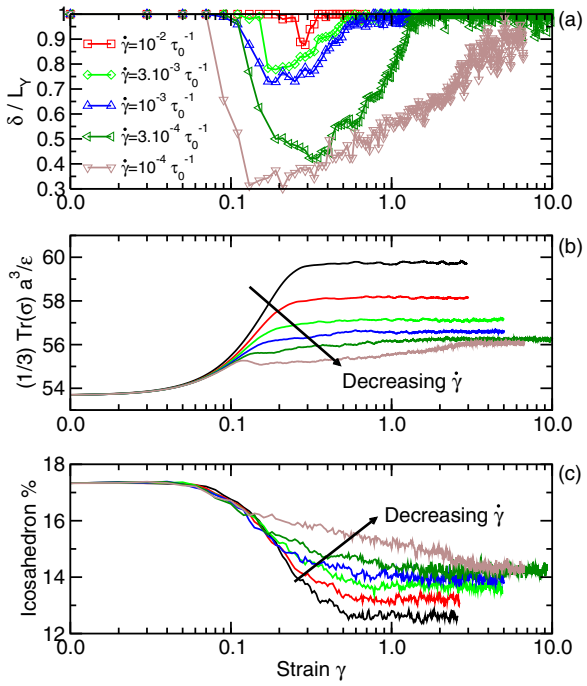

FIG. 2. (a) The width of the shear band δ/L_Y as a function of the strain γ for different shear rates, for $\phi = 0.70$ and cooling rate $\Gamma = 5 \times 10^{-4}\epsilon/(k_B\tau_0)$. The evolution of pressure in (b) and of the percentage of icosahedral packing in (c) for the same set of shear rates.

minimization. We prepare one to five independent samples for each cooling rate (one in the case of slowest Γ) and use linear oscillatory shear tests to verify that they are all initially in a rheologically solid state, well beyond the jamming point. The samples are subjected to a shear rate $\dot{\gamma}$ using Lees-Edwards boundary conditions (LEBCs) and, independently, by confining them between two walls [wall-based shearing protocol (WB)], one of which is moving at a velocity determined by the chosen rate [see also Supplemental Material (SM) [28]]. We solve equations of motion with a damping that guarantees minimal inertia effects, as discussed in Ref. [27]. The virial stress tensor is σ_{AB} [29], where $A, B \in X, Y, Z$, with X, Y, and Z corresponding to flow, gradient, and vorticity directions, respectively. All simulations used LAMMPS [30] which we modified to include size polydispersity. For all data, $\dot{\gamma}$ is in units of τ_0^{-1}.

The load curve (i.e., the shear component $\sigma \equiv \sigma_{XY}$ of the stress tensor versus the strain γ or time $= \gamma/\dot{\gamma}$) is shown in Fig. 1 for $\dot{\gamma} = 10^{-4}\tau_0^{-1}$ (LEBC). The initial elastic response at small strain is followed by a stress overshoot, after which the shear stress decays towards a steady-state value. Along the load curve [Fig. 1(a)], we reconstruct the velocity profile $\langle v_x\rangle(y)$ averaged over a strain window of $\approx 2\%$ [Fig. 1(b)], by slicing the sample along the gradient direction $\hat{y}$ and averaging the x component of the velocity over all particles (roughly 4000) in the same slice of thickness $\simeq a$ [25]. Starting from a linear velocity profile, as expected at short times (i), the shear banding initiates close to the stress overshoot (ii), where the local shear rate starts to deviate from the imposed one [Fig. 1(c)]. By the time the stress starts decaying, part of the material forms a nonflowing band and the deviation from the applied shear rate is maximum [Fig. 1(c)]. As the stress further decays (iii) we observe a backflow, similar to the unloading of an elastic material [3,17,31]. Progressive restoration of a linear profile (iv)-(v) is associated with a weak but continuous decrease of the shear stress [17] with significant fluctuations (not shown) [32].

The width δ of the flowing band (measured from the velocity profiles) depends on the applied shear rate [2,3,11,15,33]. Figure 2(a) shows δ/L_Y, for a LEBC sample, as a function of γ (where L_Y is the box dimension in the gradient direction) starting from 1 at small strains when the whole system deforms homogeneously (and elastically, as indicated by the negligible dependence on $\dot{\gamma}$), dropping to a lower value dependent on the rate, and approaching logarithmically 1 when the flow becomes homogeneous [11]. The logarithmic growth of the flowing band suggests coupling with the local aging of the nonflowing region [34,35]. The complete fluidization (i.e.,

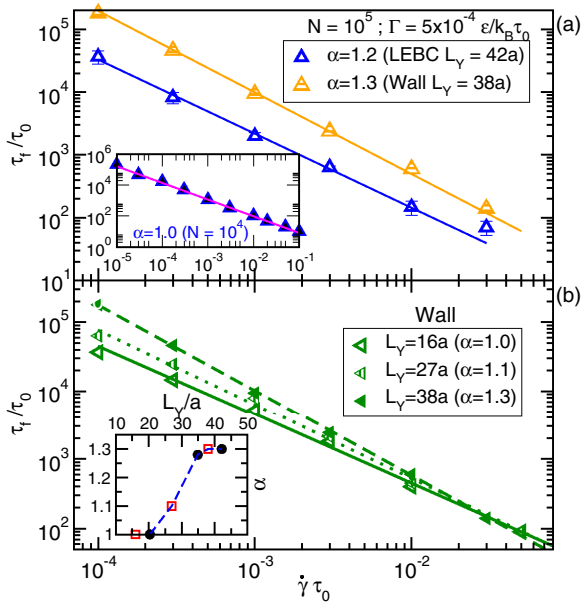

FIG. 3. Fluidization time τ_f as a function of the shear rate for $\phi = 0.70$ [$\Gamma = 5 \times 10^{-4}\epsilon/(k_B\tau_0)$]. (a) Main panel: Data for $N = 10^5$ particles, for LEBC and WB protocols. Inset: Data for $N = 10^4$ (LEBC). (b) Data for WB with different confinement lengths.

the onset of homogeneous flow) is signaled by the evolution of the normal components of the stress [the trace of the stress tensor is plotted in Fig. 2(b)], indicating that normal stresses are strongly coupled to the flow inhomogeneities [36]. Similar features are found for all LEBC and WB samples (see Ref. [28]). The fluidization time τ_f is obtained independently as the time where a linear velocity profile is recovered (within local shear rate fluctuations) and as the time where both shear and normal components of the stress tensor reach a steady state. The two estimates are consistent with each other and we use also their relative deviation to estimate error bars.

For relatively small samples ($N = 10^4$, $L_Y = 20a$), the dependence of τ_f on $\dot\gamma$ is $\tau_f \propto \dot\gamma^{-\alpha}$, with $\alpha = 1$ [Fig. 3(a) inset]. That is, the timescale needed for the complete fluidization is simply set by the imposed shear rate. For large samples ($N = 10^5, L_Y = 42a$), instead, $\alpha > 1.0$ [with $\alpha \simeq 1.3$ for both shearing protocols as shown in Fig. 3(a)], as also found in experiments [11]. The magnitudes of τ_f are larger in the WB protocol due to the wall-bulk interface (where the flow localization nucleates), but the value of α is consistent with LEBC and hence likely dictated by bulk processes. The system size dependence of α is confirmed with WB, by increasing the confinement distance in the gradient direction $\hat y$ [Fig. 3(b)]. $\alpha > 1.0$ for large enough samples indicates that the microscopic dynamical processes underlying the fluidization are not trivially slaved to the shear rate $\dot\gamma$, because they are spatially correlated over large distances that increase with the sample size. The possibility to reconcile, also in soft glassy solids, the complex phenomenology of the stress overshoot, and the yielding and banding with an underlying phase transition [37,38] is increasingly debated. Our findings hint at a nucleation process or to a critical-like growth for the flow inhomogeneities, as proposed for steady-state banding in complex fluids but here at play for a transient banding [15].

The nonflowing band is not obviously associated with shear-induced crystallization [10], phase separation [14], or any visible density gradients [39], but we find a striking link between the shear banding and a local structural signature. Through a Voronoi tessellation we obtain the statistics of polyhedra that correspond to different local packing geometries and particle coordination numbers [40]. The analysis reveals that the time evolution of the percentage of particles associated with dodecahedral Voronoi volumes (or to a icosahedral packing) is strongly correlated to the shear banding [Fig. 2(c)]. Furthermore, there is a strong spatial coupling between the banding and the organization of the icosahedrally packed particle domains: In Fig. 1(b) the dashed lines indicate the local icosahedral packing percentages along the gradient direction $\hat y$, using the same procedure employed to compute the velocity profiles, proving that, by the time the shear stresses start to relax from the overshoot, domains with mainly icosahedrally packed particles organize into the nonflowing band.

The icosahedral particle packing points to the existence of regions where the local coordination number, and hence the number of mechanical constraints on a particle, is much higher than the isostatic conditions [i.e., 6 in three dimensions (3D)] of the onset of jamming [41]. Microscopic overconstrained domains in amorphous solids allow for local compression and tension to develop under load with no net force [42]: Hence, under load, stress can be accumulated locally without necessarily changing the mechanical state of the material (e.g., yielding). Such a feature could explain why the spatial organization and the amount of icosahedrally packed domains are coupled to the emergence and persistence of the nonflowing band, consistent with the transient banding being associated with the relaxation of the stresses stored through the overshoot [3,21,43]. While the persistence of icosahedrally packed domains under shear and their participation to shear localization has also been noted in the context of locally preferred structures in supercooled liquids and glasses [44–46], here we propose that they signal overcoordinated (and hence overconstrained) regions, where stresses accumulate under load. Hence icosahedrally packed domains are akin to *self-stress states* discussed in Ref. [42].

In glassy solids and supercooled liquids with spherically symmetric potentials (as here) local icosahedral packing are energetically favored structures that geometrically frustrate long-range order [47]. Therefore by cooling a liquid sample at different rates Γ we can control the prevalence of icosahedral symmetry in the initial solid. Deeper local minima (or inherent structures) of the total potential energy are accessible upon decreasing Γ, as shown in Fig. 4(a) through the inherent structure energy per particle [48]. Deeper local minima also correspond to solids with a higher mechanical strength as measured through the storage modulus G' [Fig. 4(b)] and higher percentages of local icosahedral packing [Fig. 4(c)] [49–51]. The logarithmic increase of the stress overshoot with decreasing Γ, shown in Fig. 4(d), indicates that higher percentages of local icosahedral packing allow for a larger accumulation of stresses under deformation. The prevalence

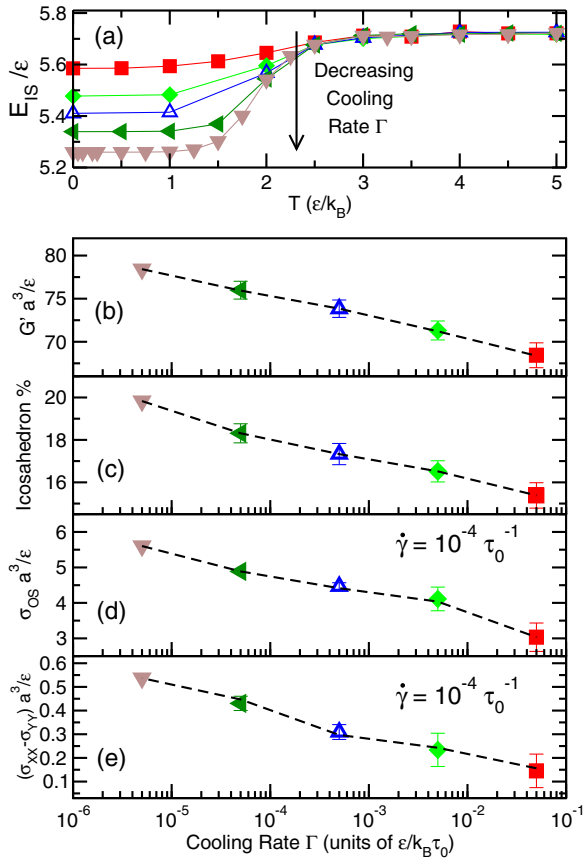

FIG. 4. (a) The inherent structure energy per particle as a function of the temperature for cooling rates $\Gamma = 5 \times 10^{-2}$ (square), 5×10^{-3} (diamond), 5×10^{-4} (up triangle), 5×10^{-5} (side triangle), and $5 \times 10^{-6} \epsilon/(k_B \tau_0)$ (down triangle). (b) Storage modulus G' and (c) percentage of icosahedral packing computed in initially solid samples as a function of Γ. (d) Stress overshoot and (e) normal stress difference computed at the stress overshoot as a function of Γ for $\dot{\gamma} = 10^{-4} \tau_0^{-1}$.

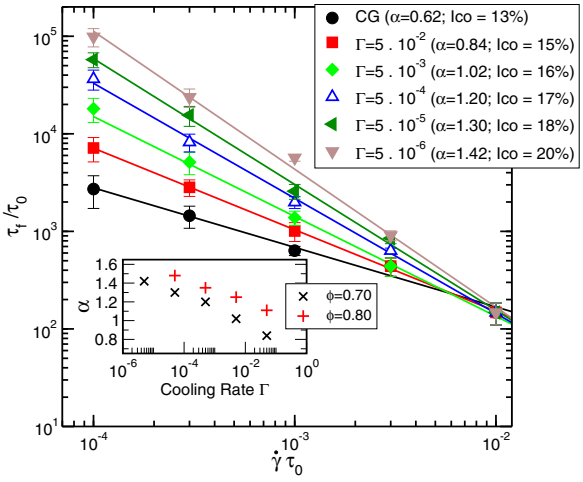

FIG. 5. Main panel: The fluidization time as a function of the shear rate (LEBC) for samples obtained from different cooling rates Γ and hence containing different percentages of icosahedral packing. The error bars are from sample-to-sample fluctuations, except for the lowest Γ where we use two independent determinations of τ_f. Inset: The fluidization exponent as a function of Γ for $\phi = 0.70$ and $\phi = 0.80$.

of icosahedral symmetry enhances the tendency of the material to dilate, as indicated by the first normal stress difference $\sigma_{XX} - \sigma_{YY}$ at the stress overshoot plotted as a function of Γ in Fig. 4(e), indicating that icosahedral packing corresponds to regions locally under compression. All findings support the idea that the icosahedrally packed domains here play the role of overconstrained domains that drive stress localization, triggering the shear banding.

By shearing at different $\dot{\gamma}$ the samples prepared at different Γ, we obtain the fluidization time τ_f as a function of $\dot{\gamma}$ in Fig. 5 (LEBC), where the fluidization exponent α increases with decreasing Γ (see Fig. 5 inset) and hence with the increasing icosahedral packing percentage in the initial sample. The value of α reach values as high as $\simeq$1.7, and for the lowest cooling rates (largest amounts of icosahedral packing) and lowest shear rates one might have to shear the samples up to strain $\gamma = 10$ to get rid of flow inhomogeneities, a scenario possibly relevant to ultrastable glasses [38]. The emerging picture is that the redistribution of the mechanical constraints under shear introduces a characteristic time that interferes with the imposed shear rate and strongly affects the timescale over which fluidization occurs.

To summarize, overconstrained domains favor stress storage (and a stress overshoot) in dense soft solids under shear, by concentrating stresses in self-stress states that are mainly compressive and that self-organize into a nonflowing band in the material. As a consequence, a complete fluidization at an imposed shear rate can only be attained by progressively redistributing constraints and eroding the nonflowing band. Such processes are responsible for the dramatic increase of the persistence of flow inhomogeneities upon decreasing the shear rate. The true steady-state behavior of the model material considered here is generic to simple yield stress fluids, well described by a Herschel-Bulkley form $\sigma - \sigma_Y \propto \dot{\gamma}^n$ (where σ_Y is the yield stress and $n \approx 0.65$) [25,52] (see SM [28]). Since overconstrained domains are a generic feature of amorphous solids, the mechanism unveiled should be relevant to yielding and shear localization in a variety of dense soft solids, well beyond the specifics of our study. Overconstrained domains may have different morphologies in different materials, not necessarily associated with dodecahedral Voronoi volumes and local icosahedral packing, but the overall physical picture will still apply.

Our results give additional input to the understanding of yielding and fluidization of dense soft solids, elucidating the role of mechanical heterogeneities and unraveling their spatiotemporal coupling with the imposed deformation. Recent mesoscopic theories rationalize the nonlinear response of dense soft solids in terms of the statistics and the spatiotemporal correlations of microscopic plastic processes [34,53,54]. Our study suggests that overconstrained domains can be the microscopic fingerprints of the mechanical heterogeneities

that those theories rely upon [20,21,43]. The connection we propose between the overconstrained domains and the concept of self-stress states for amorphous materials [42] can shed light on the dynamical and rate-dependent implications of self-stress states, beyond their current understanding, and potentially link them to the emerging plasticity in a long-sought-after unifying framework for amorphous solids. Overconstrained domains could be specifically designed into smart soft solids during solidification, to control shear localization or to tailor dynamic timescales that affect material processing, with consequences for energy costs, efficiency, and performances.

The authors thank Mehdi Bouzid, Thibaut Divoux, Craig Maloney, Xiaoming Mao, Kirsten Martens, Elian Masnada, and Peter D. Olmsted for discussions, and Georgetown University, National Science Foundation (Grant No. NSF PHY17-48958), and Swiss National Science Foundation (Grant No. PP00P2 150738) for support. This work was supported by NSF Grant No. DMR-1659532.

[1] D. Bonn, M. M. Denn, L. Berthier, T. Divoux, and S. Manneville, Rev. Mod. Phys. **89**, 035005 (2017).
[2] T. Divoux, C. Barentin, and S. Manneville, Soft Matter **7**, 9335 (2011).
[3] S. M. Fielding, Rep. Prog. Phys. **77**, 102601 (2014).
[4] T. Divoux, M. A. Fardin, S. Manneville, and S. Lerouge, Annu. Rev. Fluid Mech. **48**, 81 (2016).
[5] G. P. Shrivastav, P. Chaudhuri, and J. Horbach, J. Rheol. **60**, 835 (2016).
[6] L. Bécu, S. Manneville, and A. Colin, Phys. Rev. Lett. **96**, 138302 (2006).
[7] S. A. Rogers, D. Vlassopoulos, and P. T. Callaghan, Phys. Rev. Lett. **100**, 128304 (2008).
[8] P. Coussot and G. Ovarlez, Eur. Phys. J. E **33**, 183 (2010).
[9] R. Besseling, L. Isa, P. Ballesta, G. Petekidis, M. E. Cates, and W. C. K. Poon, Phys. Rev. Lett. **105**, 268301 (2010).
[10] L. T. Shereda, R. G. Larson, and M. J. Solomon, Phys. Rev. Lett. **105**, 228302 (2010).
[11] T. Divoux, D. Tamarii, C. Barentin, and S. Manneville, Phys. Rev. Lett. **104**, 208301 (2010).
[12] F. Varnik, L. Bocquet, and J.-L. Barrat, J. Chem. Phys. **120**, 2788 (2004).
[13] V. Chikkadi, D. M. Miedema, M. T. Dang, B. Nienhuis, and P. Schall, Phys. Rev. Lett. **113**, 208301 (2014).
[14] E. Irani, P. Chaudhuri, and C. Heussinger, Phys. Rev. Lett. **112**, 188303 (2014).
[15] P. D. Olmsted, Rheol. Acta **47**, 283 (2008).
[16] J. M. Adams and P. D. Olmsted, Phys. Rev. Lett. **102**, 067801 (2009).
[17] J. M. Adams, S. M. Fielding, and P. D. Olmsted, J. Rheol. **55**, 1007 (2011).
[18] A. R. Hinkle and M. L. Falk, J. Rheol. **60**, 873 (2016).
[19] A. Nicolas, J.-L. Barrat, and J. Rottler, Phys. Rev. Lett. **116**, 058303 (2016).
[20] K. Martens, L. Bocquet, and J.-L. Barrat, Soft Matter **8**, 4197 (2012).
[21] F. Puosi, J. Olivier, and K. Martens, Soft Matter **11**, 7639 (2015).
[22] A. Barbot, M. Lerbinger, A. Hernandez-Garcia, R. García-García, M. L. Falk, D. Vandembroucq, and S. Patinet, Phys. Rev. E **97**, 033001 (2018).
[23] J. D. Weeks, D. Chandler, and H. C. Andersen, J. Chem. Phys. **54**, 5237 (1971).
[24] F. Varnik, L. Bocquet, J.-L. Barrat, and L. Berthier, Phys. Rev. Lett. **90**, 095702 (2003).
[25] V. V. Vasisht, S. K. Dutta, E. Del Gado, and D. L. Blair, Phys. Rev. Lett. **120**, 018001 (2018).
[26] V. V. Vasisht, M. L. Goff, K. Martens, and J.-L. Barrat, arXiv:1812.03948.
[27] V. V. Vasisht and E. Del Gado, arXiv:1908.03943 [Phys. Rev. E (to be published)].
[28] See Supplemental Material at http://link.aps.org/supplemental/10.1103/PhysRevE.102.010604 for additional data obtained with the wall-based (WB) protocol and for the flow curves.
[29] J. H. Irving and J. G. Kirkwood, J. Chem. Phys. **18**, 817 (1950).
[30] S. Plimpton, J. Comput. Phys. **117**, 1 (1995).
[31] O. S. Agimelen and P. D. Olmsted, Phys. Rev. Lett. **110**, 204503 (2013).
[32] S. Majumdar and A. K. Sood, Phys. Rev. Lett. **101**, 078301 (2008).
[33] M. L. Manning, E. G. Daub, J. S. Langer, and J. M. Carlson, Phys. Rev. E **79**, 016110 (2009).
[34] C. Derec, A. Ajdari, and F. Lequeux, Eur. Phys. J. E **4**, 355 (2001).
[35] A. Pons, A. Amon, T. Darnige, J. Crassous, and E. Clément, Phys. Rev. E **92**, 020201(R) (2015).
[36] J. Rottler and M. O. Robbins, Phys. Rev. E **68**, 011507 (2003).
[37] R. L. Moorcroft, M. E. Cates, and S. M. Fielding, Phys. Rev. Lett. **106**, 055502 (2011).
[38] M. Ozawa, L. Berthier, G. Biroli, A. Rosso, and G. Tarjus, Proc. Natl. Acad. Sci. USA **115**, 6656 (2018).
[39] J. K. Dhont and W. J. Briels, Rheol. Acta **47**, 257 (2008).
[40] B. J. Gellatly and J. L. Finney, J. Non-Cryst. Solids **50**, 313 (1982).
[41] M. Wyart, S. R. Nagel, and T. A. Witten, Europhys. Lett. **72**, 486 (2005).
[42] T. C. Lubensky, C. L. Kane, X. Mao, A. Souslov, and K. Sun, Rep. Prog. Phys. **78**, 073901 (2015).
[43] S. Patinet, D. Vandembroucq, and M. L. Falk, Phys. Rev. Lett. **117**, 045501 (2016).
[44] D. Rodney and T. Schrøder, Eur. Phys. J. E **34**, 1 (2011).
[45] R. Pinney, T. B. Liverpool, and C. P. Royall, J. Chem. Phys. **145**, 234501 (2016).
[46] C. Zhang, N. Gnan, T. G. Mason, E. Zaccarelli, and F. Scheffold, J. Stat. Mech.: Theory Exp. (2016) 094003.
[47] P. J. Steinhardt, D. R. Nelson, and M. Ronchetti, Phys. Rev. Lett. **47**, 1297 (1981).
[48] S. Sastry, P. G. Debenedetti, and F. H. Stillinger, Nature (London) **393**, 554 (1998).

[49] M. Mosayebi, E. Del Gado, P. Ilg, and H. C. Öttinger, J. Chem. Phys. **137**, 024504 (2012).
[50] C. P. Royall and S. R. Williams, Phys. Rep. **560**, 1 (2015).
[51] P. Ronceray and P. Harrowell, Soft Matter **11**, 3322 (2015).
[52] P. Hébraud and F. Lequeux, Phys. Rev. Lett. **81**, 2934 (1998).
[53] A. Nicolas, E. E. Ferrero, K. Martens, and J.-L. Barrat, Rev. Mod. Phys. **90**, 045006 (2018).
[54] R. Benzi, T. Divoux, C. Barentin, S. Manneville, M. Sbragaglia, and F. Toschi, Phys. Rev. Lett. **123**, 248001 (2019).

Correction: The omission of a support statement in the Acknowledgments has been fixed.